JOURNAL OF MATERIALS SCIENCE 22 (1987) 37–45

Linear analytical theory of a transformation from a single crystal A to another single crystal B

G. E. W. SCHULZE, H.-P. WILBERT
Abt. Werkstoffwissenschaft des Physikalischen Instituts der Universität Düsseldorf, Bundesrepublik Deutschland, FRG

An isothermal phase transformation from a single crystal A to another single crystal B is theoretically investigated along preferred lines (Rosiwal's lines). It is supposed that the nuclei of the B-phase are Poisson distributed within the single crystal A. From these nuclei the B-grains grow instantaneously, equioriented, and in the form of cuboids with three different growth rates v_x, v_y and v_z. If the B-grains touch, growth stops and they form a larger B-grain. We derive for this microstructure, at time t along the three Rosiwal's lines (X-line, Y-line, Z-line), the distribution densities of the lengths of the A-phases as well as of the B-phases using the theory of probability. The two-dimensional model ($z = 0$) is considered in detail, idealizing the transformation within a thin layer.

1. Introduction

1.1 Motivation

The same cut of a transforming layer, from the homeotropic nematic phase to the smectic B-phase, is shown at two different times in Figs 1a and b. The layer with a thickness of about 10 μm lies between slides representing approximately a two-dimensional microstructure. The equioriented B-grains grow almost exclusively in one direction. (Further details are given in [1].) Investigations of other substances have shown a growth of rectangular grains in both directions.

These experimental investigations lead to the problem of the theoretical characterization of the microstructure of an isothermic and anisotropic transforming one-componentic layer at time t, containing the passing and the forming phases. In order to solve this problem we have created a two-dimensional model of idealized nucleation and crystal growth defining the microstructure at each time t during transformation in a statistically complete form.

1.2. Two-dimensional model (2-D model)

The microstructure at time t is defined by the following assumptions:

1. The single crystal A, at time $t = 0$, occupies only two dimensions and is infinitely extended. (This assumption simplifies the mathematical treatment.)
2. Nuclei of the B-phase are Poisson distributed (independently and randomly) within the A-phase at time $t = 0$, with a mean number of n nuclei per area unit.
3. All grains of the B-phase instantaneously start to grow at time $t = 0$ from their nuclei in the form of identical, parallel orientated rectangles (see Fig. 2). The linear growth rates are v_x and v_y.
4. If two B-grains touch, they coalesce to form a larger, single crystalline B-grain (which contains no B–B grain boundary).
5. During phase transformation no new nuclei are formed and no shrinking occurs.

The following values in generalized units are used for graphical illustration of the transformation: $n = 1$; $v_x = 1$; $v_y = 0.5$. These chosen values are used in Figs 4, 5, 7, 8 and 10. We additionally used $t = 0.5$ to illustrate a fixed microstructure; this chosen value is used in Figs 2, 3, 6, 9 and 11. An expansion from two to three dimensions is given in Sections 4, 5 and 6.

1.3. Linear analytical characterization of the microstructure at time t

Microstructures are characterized in the field of quantitative microscopy [2–5]. Here the linear analysis is a common method, characterizing the microstructure in one dimension: a line (Rosiwal's line) is drawn parallel to a preferred direction, e.g. the X-line parallel to the greatest growth rate, v_x. Along this X-line alternating A- and B-phases occur with their different lengths a and b, respectively (see Figs 3a and c). Therefore the following quantities and functions exist along the X-line at time t:

mean number, N, of intervals of A-phases as well as of B-phases per unit length;
length fraction, F, of the B-phase;
distribution density $h(a)$ of the lengths a of the A-phase;
distribution density $i(b)$ of the lengths b of the B-phase.

As shown in the field of quantitative microscopy, each

0022–2461/87 $03.00 + .12

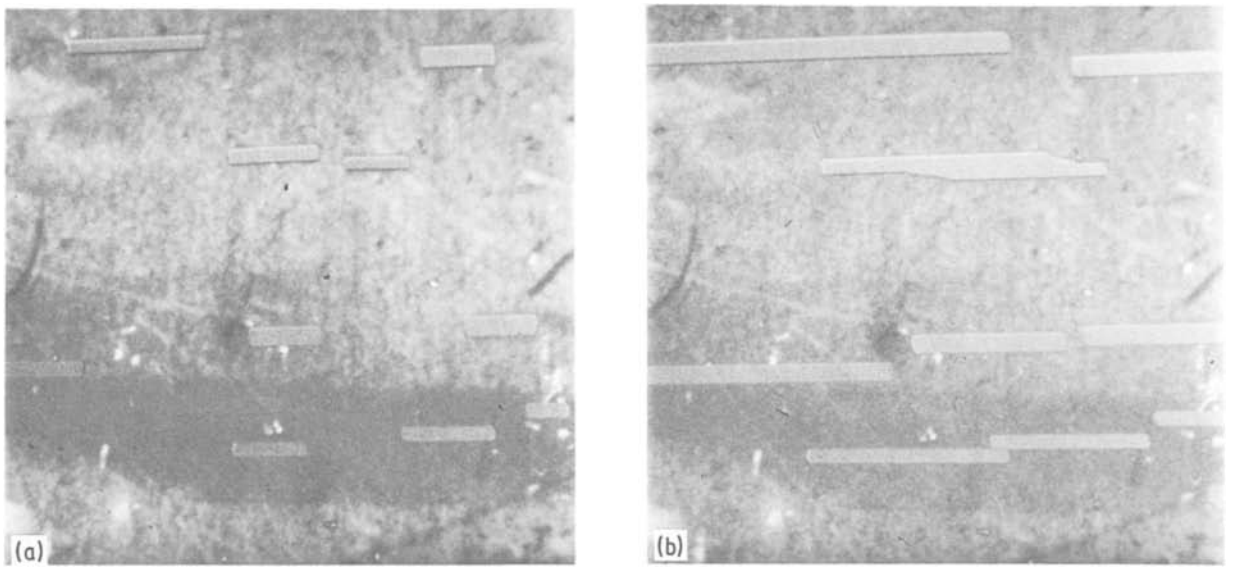

Figure 1 (a) Microphotography of a layer between crossed polarizers. The layer consists of a nearly homeotropic phase A, containing ten parallel oriented rods like grains of phase B. (b) The same cut as Fig. 1a, but a little later. The width of the photographs equals 0.2 mm in the sample.

arbitrary infinite line parallel to the X-line used yields the same statistical results.

1.4. Aims

In the following sections $N(t)$, $F(t)$, $h(a; t)$, and $i(b; t)$ of the microstructure at time t are derived by used of the theory of probability. The 1-D model has been completely derived in a previous work [6], and further 2-D and 3-D models have been investigated in [7].

2. Microstructure of the 2-D model along the X-line at time t

2.1. Virtual nuclei

We consider a strip along the X-line, limited by parallel straight lines with a distance $v_y t$ from the X-line, as shown in Fig. 3a. At time t all nuclei outside the strip cannot, on principle, reach the X-line with their grains. These nuclei are called "no potential nuclei". All nuclei within the strip at time t can (but do not have to) reach the X-line with their grains. These nuclei are called "potential nuclei".

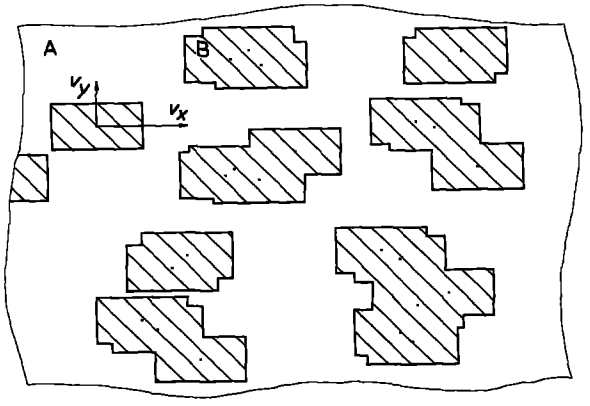

Figure 2 Two-dimensional microstructure. The points represent the nuclei. The shaded areas represent the single crystalline B-phases. v_x and v_y are the linear growth rates. We choose $n = 1$, $v_x = 1$, $v_y = 0.5$, $t = 0.5$.

The rectangular projection of all potential nuclei upon the X-line yields the "virtual nuclei", as shown in Fig. 3b. As supposed, all nuclei within the 2-D model are Poisson distributed, and consequently the potential nuclei (within the strip) are also Poisson distributed. Therefore their x-coordinates have to be Poisson distrubuted (randomly, independently) along the X-line, which means that the virtual nuclei are also Poisson distributed along the X-line.

The mean number of virtual nuclei per length unit along the X-line at time t, n_x, follows from

$$n_x = 2v_y tn. \tag{1}$$

In the theory of probability [8], for Poisson distributed points along a line with a mean number n_x of points per length unit, the distance x between two neighbouring points is exponentially distributed with a distribution density

$$j(x) = n_x \exp(-n_x x). \tag{2}$$

It is true that

$$\int_{x=0}^{\infty} j(x)\,\mathrm{d}x = 1 \quad \text{(normalization)}, \tag{3}$$

and that

$$\int_{x=0}^{\infty} x\, j(x)\,\mathrm{d}x = \bar{x} = 1/n_x$$

(mean distance between neighbouring points). (4)

Therefore the distribution density j of the distance x between neighbouring virtual nuclei along the X-line at time t is given by

$$j(x; t) = \begin{cases} 0 & \text{for } x < 0 \\ 2nv_y t \exp(-2nv_y t\, x) & \text{for } x \geqslant 0 \end{cases} \tag{5}$$

Fig. 3b shows some x-distances along the X-line.

2.2. Derivation of $N(t)$

The length of each B-grain grown unhindered along

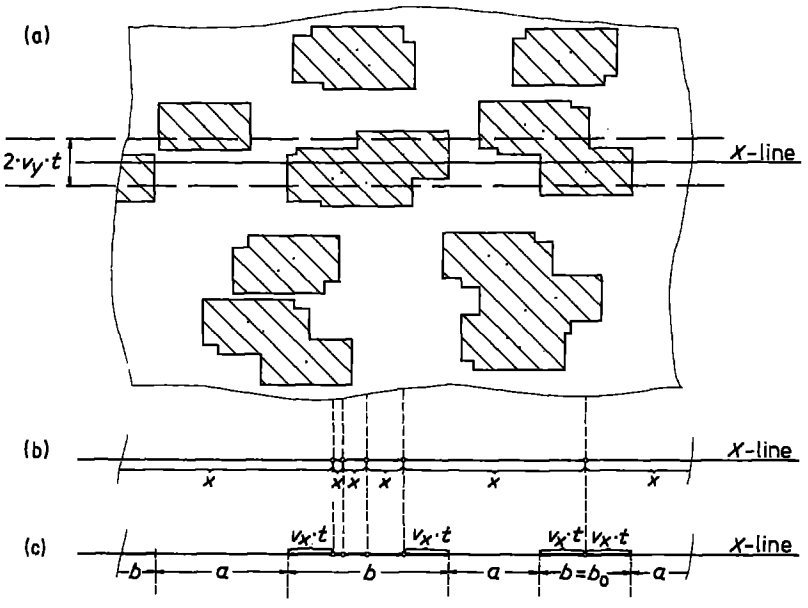

Figure 3 (a) The same microstructure as in Fig. 2, containing Rosiwal's line (X-line) and its strip with a width of $2v_y t$. The points within the strip represent the potential nuclei. A-phase and B-phase alternate along the X-line. (b) X-line containing virtual nuclei. The x-distances are the lengths between two neighbouring virtual nuclei. (c) X-line containing A-phases with different lengths a and B-phases (B-lengths) with different lengths b. The B-phase with a length b ($> b_0$) contains four virtual nuclei. The B-phase with the length b_0 contains only one virtual nucleus.

the X-line at time t amounts to

$$b_0 = 2v_x t, \tag{6}$$

where b_0 is the shortest length of the B-phases at time t on the X-line (see Fig. 3c).

By use of Figs 3a–c, we see that each distance x between neighbouring virtual nuclei with $x < b_0$ has transformed. Therefore it represents a part of the length b of a B-phase. Distance $x \geqslant b_0$ contains B-phase on its left as well as on its right side, each with a length of $v_x t$. Furthermore this x-interval contains in its centre the A-phase with a length of

$$a = x - b_0, \tag{7}$$

being symmetrically arranged.

The fraction, W, of these A-intervals with respect to all x-intervals on the X-line is given by

$$W(t) = \int_{x=b_0}^{\infty} j(x)\, dx = \exp(-n_x b_0) = \exp(-4nv_x v_y t^2) \tag{8}$$

Therefore the mean number of A-intervals per length unit along the X-line, N, is given by

$$N(t) = n_x W(t) = 2nv_y t \exp(-4nv_x v_y t^2) \tag{9}$$

Fig. 4 shows the graph $N(t)$ for the example given above.

At $t = 0$, phase-A only exists and therefore $N = 0$. The shape of $N(t)$ is caused by two effects: the arrival of new grains on the X-line dominates before the maximum of N is reached, and therefore the number of N increases. Beyond the maximum the coalescence of grains dominate and therefore the number of A-intervals decreases. Finally only B-phase exists, and we have $N = 0$. The mean number of B-phases per unit length also equals $N(t)$.

The differentiation of $N(t)$ with respect to time t gives

$$\dot{N}(t) = 2nv_y \exp(-4nv_x v_y t^2)(1 - 8nv_x v_y t^2) \tag{10}$$

Fig. 5 shows $\dot{N}(t)$; $\dot{N}(t) = 0$ is reached at

$$t = (8nv_x v_y)^{-1/2} = 0.5. \tag{11}$$

At this time we obtain the maximum of $N(t)$ in Fig. 4.

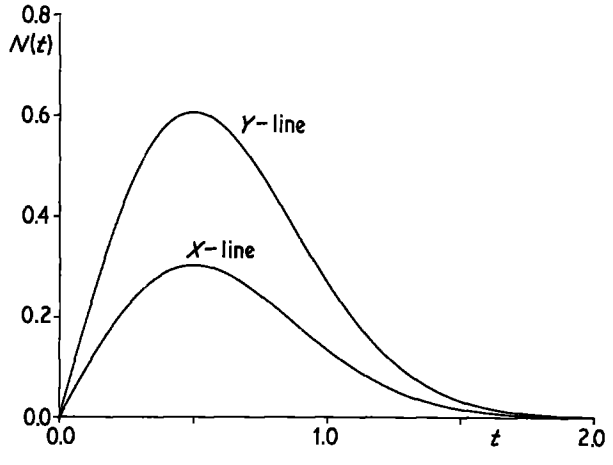

Figure 4 $N(t)$ represents the number of A-phases (or B-phases) per unit length along the X-line and along the Y-line. For the latter see Section 3.

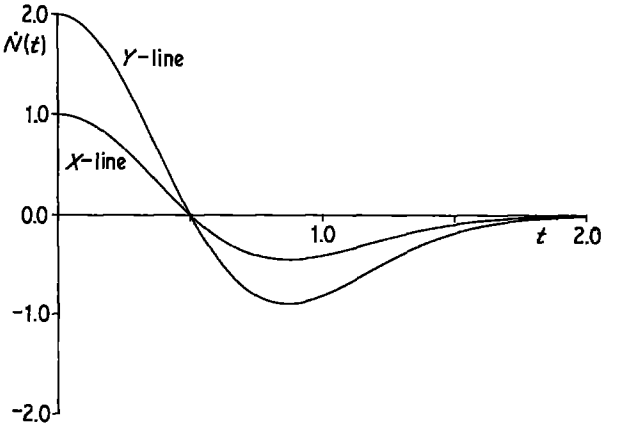

Figure 5 $\dot{N}(t)$ represents the derivation of N with respect to t along the X-line and along the Y-line.

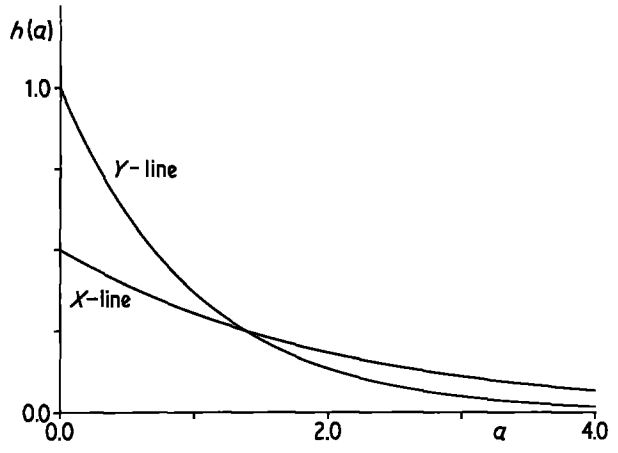

Figure 6 Distribution density h of the length a along the X-line and along the Y-line at $t = 0.5$, $F = 0.39$.

2.3. Derivation of $h(a)$

From Equations 2, 7, 8, 1 and 6 we obtain the normalized distribution density h of the length a of the A-phases at time t:

$$h(a; t) = \frac{n_x \exp[-n_x(a + b_0)]}{W(t)} = 2nv_y t \exp(-2v_y t\, a) \quad (12)$$

Fig. 6 shows $h(a; 0.5)$. The mean value $\bar{a}$ of the lengths a at t is given by

$$\bar{a} = \frac{1}{(2nv_y t)} \quad (13)$$

Since $h(a; t) = j(x; t)$, we have $\bar{a} = \bar{x}$. Each snapshot of the microstructure yields an exponential distribution of the a-lengths. $\bar{a}$ decreases proportionally to $1/t$.

2.4. Avrami relation

The length fraction, M, of phase-A along the X-line at time t, equals the part M of A-phase per unit length. It is given by

$$M(t) = \bar{a}\, N(t). \quad (14)$$

With Equations 8 and 9 we obtain

$$M(t) = W(t) \quad (15)$$

The complementary part of B-phase per unit length along the X-line at time t, F, meaning the length fraction of the B-phase, is given by

$$F(t) = 1 - M(t) = 1 - \exp(-4nv_x v_y t^2) \quad (16)$$

Fig. 7 shows $F(t)$ with its point of inflection at $t = 0.5$. Differentiation yields

$$\dot{F}(t) = -\dot{M}(t) = -\dot{W}(t) = 8nv_x v_y t \exp(-4nv_x v_y t^2) = 4v_x N(t). \quad (17)$$

By quantitative microscopy for the B-phase, it is proved that the length fraction along the X-line equals the areal fraction within the x–y plane. Therefore the $F(t)$ in Equation 16 represents also the "fraction transformed" in the two-dimensional microstructure under consideration. Equation 16 is often called the "Avrami relation". The proportionality of $\dot{F}(t)$ and $N(t)$ from Equation 17 is physically understandable because on the one hand the interphase interfaces are the centres of growth along the X-line, and on the other hand the mean number of interphase interfaces along the X-line amounts to $2N(t)$.

2.5. Class 1 B-lengths

A B-length on the X-line containing only one virtual nucleus is called a "class 1 B-length". Its length b amounts to $b_0 = 2v_x t$ at time t along the X-line. Therefore the (normalized) distribution density $i_1(b; t)$ of the length b is a delta function:

$$i_1(b; t) = \delta(b - b_0) = \delta(b - 2v_x t). \quad (18)$$

The mean number of class 1 B-lengths per unit length along the X-line at time t, N_1, is derived as follows. The probability of obtaining an x-interval with $x > b_0$ amounts to W, as given by Equation 8. If two such x-intervals are neighbours, we have a class 1 B-length. This event has the probability $W \cdot W$, because the two x-lengths are independent of each other. Therefore the mean number of class 1 B-lengths amounts to

$$N_1(t) = n_x W^2(t). \quad (19)$$

Fig. 8 shows $N_1(t)$. The fraction $N_1(t)/N(t)$ amounts to $W(t)$ (see Fig. 7).

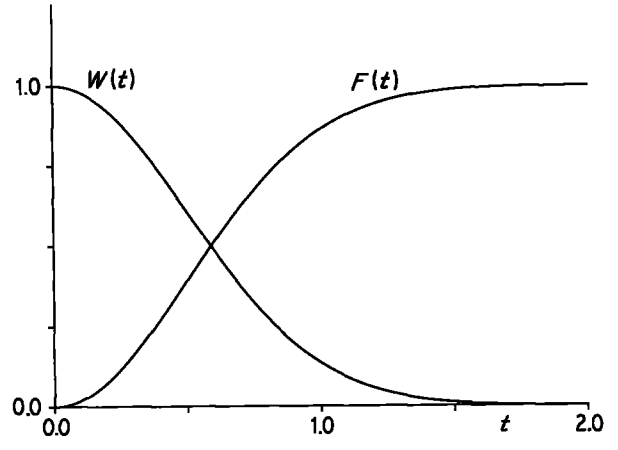

Figure 7 Fraction transformed, $F(t)$, and fraction of A-phase, $W(t)$.

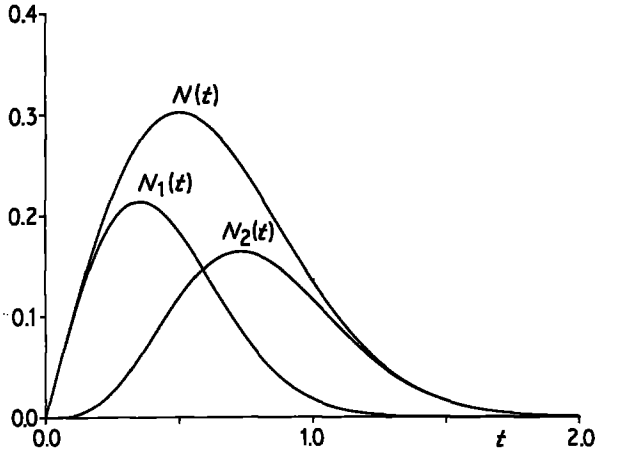

Figure 8 N_1 is the mean number of class 1 B-lengths per unit length along the X-line. N_2 is the mean number of class 2 B-lengths per unit length along the X-line. N is the sum of N_1 and N_2.

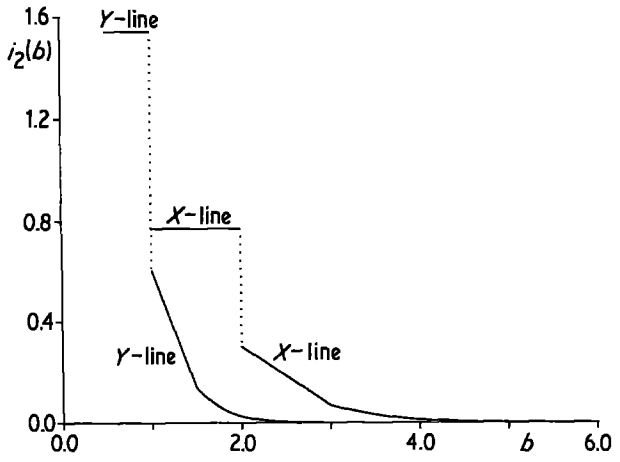

Figure 9 Distribution density $i_2(b; t)$ of the length b of the class 2 B-lengths at time $t = 0.5$ along the X-line and along the Y-line. $F = 0.39$.

2.6. Class 2 B-lengths

A B-length on the X-line containing two or more virtual nuclei is called a "class 2 B-length". Its length b is a random variable and its value is greater than b_0. The normalized distribution density $i_2(b, t)$ of the lengths b of the class 2 B-lengths is defined by

$$i_2(b; t) = \frac{n_x}{[\exp(n_x b_0) - 1]} \times \begin{cases} 0 & \text{for } 0 < b \leqslant b_0 \\ 1 & \text{for } b_0 < b \leqslant b_0 \cdot 2 \\ g(b; t, K) & \text{for } Kb_0 < b \leqslant b_0(K+1) \end{cases} \quad (20)$$

with $K = 2, 3, 4, \ldots$ and with

$$g(b; t, K) = 1 + \sum_{j=1}^{K-1} (-n_x)^j \exp(-jn_x b_0) \times \{[b - (j+1)b_0]^j/j! + [b - (j+1)b_0]^{j-1}/[n_x(j-1)!]\} \quad (21)$$

and with the abbreviations

$$b_0 = 2v_x t \text{ and } n_x = 2nv_y t.$$

The derivation is a bit lengthy and therefore it will be given in a later paper [9]. Fig. 9 shows $i_2(b; 0.5)$ along the X-line. The smallest length of a class 2 B-length amounts to b_0 (= 1). The discontinuity of $i_2(b; 0.5)$ at $b = 2$ is caused by the abrupt vanishing of class 2 B-lengths with only two virtual nuclei. The salient point of i_2 at $b = 3$ is caused by vanishing of class 2 B-lengths containing three virtual nuclei only. For $b > 3$ the i_2 is continuous and differentiable. A similar discussion has been given in [6]. The mean number of class 2 B-lengths per unit length along the X-line at time t, N_2, follows from

$$N_2 = N - N_1 = n_x W - n_x W^2 = 2nv_y t \exp(-4nv_x v_y t^2)[1 - \exp(-4nv_x v_y t^2)]. \quad (22)$$

Fig. 8 shows $N_2(t)$. $N_1(t)$ and $N_2(t)$ intersect at $F = 0.5$, where $F(t)$ and $W(t)$ in Fig. 7 also intersect.

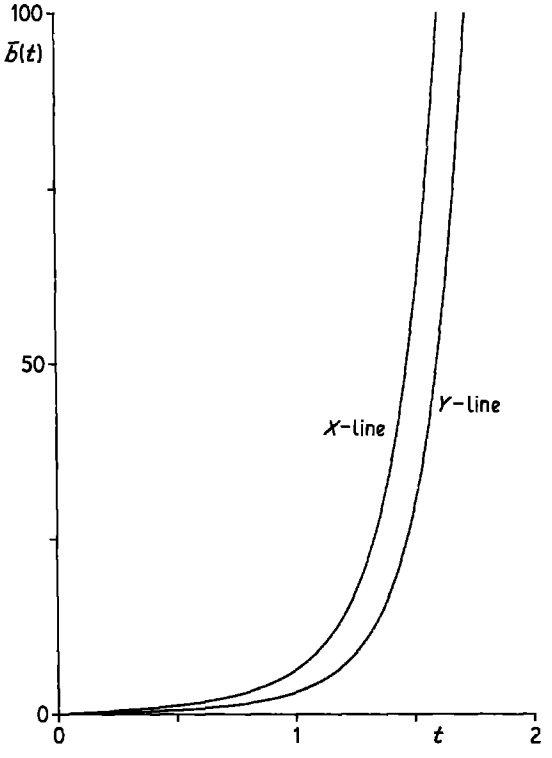

Figure 10 Mean length $\bar{b}(t)$ of the B-phases along the X- and along the Y-line.

The fraction $N_2(t)/N(t)$ amounts to $F(t)$ (see Fig. 7). The mean length $\bar{b}_2(t)$ of the class 2 B-lengths at time t follows from

$$\bar{b}_2(t) = (F - N_1 b_0)/N_2. \quad (23)$$

2.7. Density distribution $i(b; t)$

The length unit on the X-line at time t contains N lengths of the A- as well as the B-phase. Therefore we have

$$N(\bar{a} + \bar{b}) = 1. \quad (24)$$

From this equation we compute the mean length $\bar{b}$ of all B-lengths:

$$\bar{b} = 1/N - \bar{a} = (2nv_y t)^{-1} \times [\exp(+4nv_x v_y t^2) - 1]. \quad (25)$$

Fig. 10 shows $\bar{b}(t)$ with $\bar{b}(0) = 0$ and $\bar{b}(\infty) = \infty$. The normalized density distribution $i(b; t)$ of the length b of all B-lengths along the X-line at time t is given by use of Equations 18 and 20 as

$$i(b; t) = \begin{cases} 0 & \text{for } b < b_0 \\ i_1(b; t)W & \text{for } b = b_0 \\ i_2(b; t)(1 - W) & \text{for } b > b_0. \end{cases} \quad (26)$$

3. Microstructure of the 2-D model along the Y-line at time t

3.1. Strip parallel to the Y-line

Fig. 11 shows Rosiwal's line parallel to the Y-direction through the microstructure seen above in Fig. 2. Now the strip shows a width of $2v_x t$, containing all potential nuclei with respect to the Y-line. The mean number of virtual nuclei per unit length at

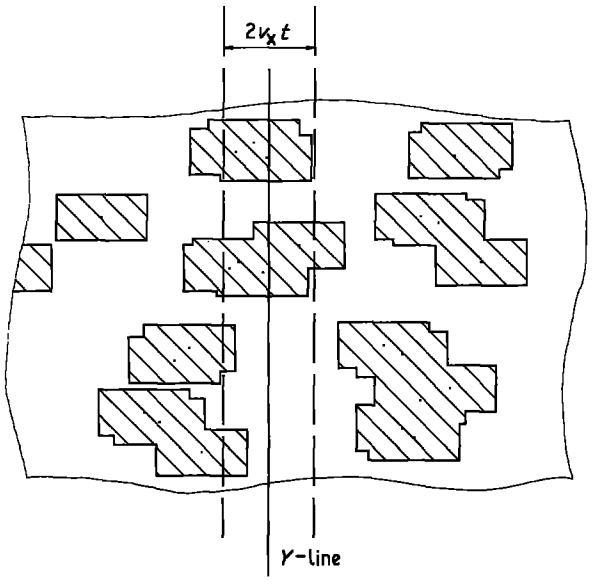

Figure 11 The microstructure from Fig. 2, containing a Y-line and its strip with a width of $2v_x t = 1$.

time t along the Y-line, n_y, amounts to

$$n_y = 2nv_x t. \tag{27}$$

The length b_0 of the grains of class 1 amounts to

$$b_0 = 2v_y t. \tag{28}$$

3.2. Results

All derivations and results given in Section 2 for the linear analysis along the X-line are valid for the linear analysis along the Y-line, if we interchange v_x and v_y.

The following quantities and their derivations with respect to time t are invariant after interchange: $W(t)$ (Equation 8), $F(t)$ (Equation 16), $M(t)$ (Equation 16).

The following quantities are altered by interchange of v_x and v_y: b_0, $\bar{x}$, $j(x)$ (Fig. 6), $N(t)$ (Fig. 4), $\dot{N}(t)$ (Fig. 5), $h(a)$ (Fig. 6), $\bar{a}$, $i_1(b)$, $N_1(t)$ (Fig. 8), $i_2(b)$ (Fig. 9), $N_2(t)$ (Fig. 8), $\bar{b}$ (Fig. 10), $i(b)$.

4. Theory of linear analysis of the 3-D model

4.1. 3-D model

We expand the 2-D model, given in Section 1.2, for the space (3-D) model in the following way. The nuclei are Poisson distributed within the space with a mean number of n nuclei per unit volume. Each crystal grows in three directions with the rates v_x, v_y and v_z. The form of each unhindered growing B-grain at time t is a cuboid with the three lengths $2v_x t$, $2v_y t$, $2v_z t$. As an illustration we also use $v_z = 0.2$.

4.2. Potential nuclei

Now the potential nuclei are contained within a tube. The central line of the tube represents the X-line, as shown in Fig. 12. This tube has rectangular cross-section with an area amounting to $2v_y t\ 2v_z t$.

The virtual nuclei are again Poisson distributed. The mean number of virtual nuclei per unit length along the X-line at time t is given by

$$n_x = 4nv_y v_z t^2 \tag{29}$$

4.3. Quantities along the X-line

The quantities of the 3-D model are derived in the same way as given in Section 2 for the 2-D model, and are listed below.

$$\begin{aligned}
b_0(t) &= 2v_x t \\
\bar{x}(t) &= 1/(4nv_y v_z t^2) \\
j(x) &= 4nv_y v_z t^2 \exp(-4nv_y v_z t^2 x) \\
W(t) &= \exp(-8nv_x v_y v_z t^3) \\
N(t) &= 4nv_y v_z t^2 \exp(-8nv_x v_y v_z t^3) \\
\dot{N}(t) &= 8nv_y v_z t \exp(-8nv_x v_y v_z t^3) \\
&\quad \times (1 - 12nv_x v_y v_z t^3) \\
h(a) &= 4nv_y v_z t^2 \exp(-4nv_y v_z t^2 a) \\
\bar{a} &= 1/(4nv_y v_z t^2) \\
F(t) &= 1 - \exp(-8nv_x v_y v_z t^3) \\
i_1(b) &= \delta(b - 2v_x t) \\
N_1(t) &= 4nv_y v_z t^2 \exp(-16nv_x v_y v_z t^3) \\
N_2(t) &= 4nv_y v_z t^2 \exp(-8nv_x v_y v_z t^3) \\
&\quad \times [1 - \exp(-8nv_x v_y v_z t^3)]
\end{aligned}$$

$$i_2(b) = \frac{4nv_y v_z t^2}{\exp(-8nv_x v_y v_z t^3) - 1} \times \begin{cases} 0 & \text{for } 0 < b \leqslant 2v_x t \\ 1 & \text{for } 2v_x t < b \leqslant 2 \times 2v_x t \\ g(b;\, t,\, K) & \text{for } K2v_x t < b \leqslant (K+1)2v_x t \end{cases}$$

with $K = 2, 3, 4, \ldots$ and with

$$g(b;\, t,\, K) = 1 + \sum_{j=1}^{K-1} (-4nv_y v_z t^2)^j \exp(-j8nv_x v_y v_z t^3) \left\{ \frac{[b - (j+1)2v_x t]^j}{j!} + \frac{[b - (j+1)2v_x t]^{(j-1)}}{4nv_y v_z t^2\,(j-1)!} \right\}$$

$$\bar{b}(t) = \frac{\exp(8nv_x v_y v_z t^3) - 1}{4nv_y v_z t^2}$$

$$i(b) = \begin{cases} 0 & \text{for } b < 2v_x t \\ \exp(-8nv_x v_y v_z t^3)\ \delta(b - 2v_x t) & \text{for } b = 2v_x t \\ [1 - \exp(-8nv_x v_y v_z t^3)]\ i_2(b) & \text{for } b > 2v_x t \end{cases}$$

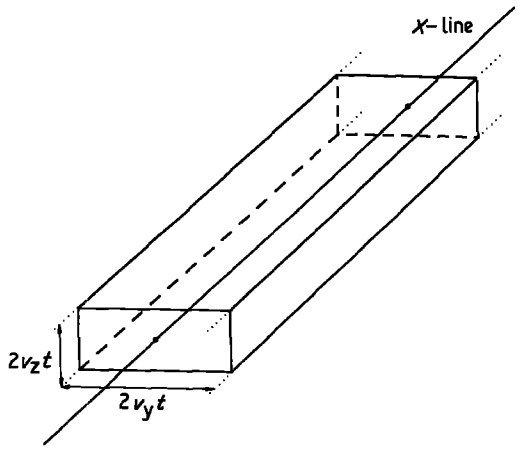

Figure 12 Tube with the cross-section 0.5 × 0.2. The central line represents the X-line through the 3-D model.

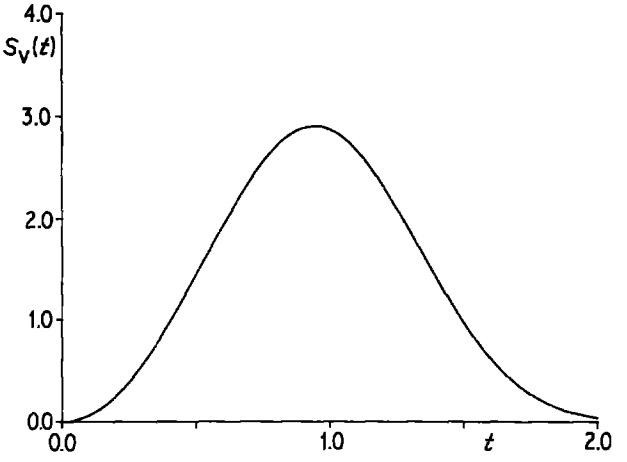

Figure 13 Mean area of interphase interfaces per unit volume, $S_V(t)$.

4.4. Quantities along the Y-line and the Z-line

The results along the Y-line are obtained if we replace v_x by v_y and v_y by v_x in Section 4.3. The results along the Z-line are obtained if we replace v_x by v_z and v_z by v_x.

The quantities $W(t)$, $M(t)$, $F(t)$, as well as their derivations with respect to time t, stay invariant after this interchange. They are also measured in the field of quantitative microscopy by the point analysis.

4.5. S_V and interphase interfacial energy

The mean number of A–B interfaces per unit length along the X-line at time t amounts to $2N(t)$, because there are N B-phases each with two interfaces. Consequently the mean area of y–z interphase interfaces within a unit cube is also given by $2N(t)$. We use indices in order to distinguish the three main directions. The mean area of interphase interface per unit volume, S_V, follows from

$$S_V = 2(N_x + N_y + N_z)$$
$$= 8nt^2(v_y v_z + v_z v_x + v_x v_y) \exp(-8nv_x v_y v_z t^3) \quad (30)$$

Fig. 13 shows $S_V(t)$ with $n = 1$; $v_x = 1$; $v_y = 0.5$; $v_z = 0.2$. The maximum of $S_V(t)$ is reached at $t_{max} = 0.941\ldots$. At the same time $\dot{F}$ reaches its maximum.

d_{xy} may be the specific interphase interfacial energy of an xy-boundary. Analogously we define d_{yz} and d_{zx}. The mean interphase interfacial energy per unit volume of the 3-D model at time t, $E(t)$, is given by

$$E(t) = 8nt^2(d_{xy}v_x v_y + d_{yz}v_y v_z + d_{zx}v_z v_x)$$
$$\times \exp(-8nv_x v_y v_z t^3) \quad (31)$$

5. Theory of linear analysis of the 3-D surface model

5.1. 3-D surface model and potential nuclei

Experimental linear analysis is often done on the surface of the sample. The usual model is the "3-D surface model", defined to be a 3-D model within the infinite half-space for all x and all y values, but only for $z \leqslant 0$. Now we investigate the microstructure of the xy-plane along the X-line at time t. As shown in Fig. 14, the potential nuclei are situated within a half tube with the cross-section of $2v_y t v_z t$. The mean number of virtual nuclei per unit length on the X-line at time t, n_x, amounts to

$$n_x = 2nv_y v_z t^2 = 1/\bar{x}. \quad (32)$$

5.2. Quantities along the X-line

The quantities of the 3-D surface model are derived in the same way as given in Section 2 for the 2-D model, and are listed below.

$$b_0(t) = 2v_x t$$
$$\bar{x}(t) = 1/(2nv_y v_z t^2)$$
$$j(x) = 2nv_y v_z t^2 \exp(-2nv_y v_z t^2 x)$$
$$W(t) = \exp(-4nv_x v_y v_z t^3)$$
$$N(t) = 2nv_y v_z t^2 \exp(-4nv_x v_y v_z t^3)$$
$$\dot{N}(t) = 4nv_y v_z t \exp(-4nv_x v_y v_z t^3)$$
$$\times (1 - 6nv_x v_y v_z t^3)$$
$$h(a) = 2nv_y v_z t^2 \exp(-2nv_y v_z t^2 a)$$
$$\bar{a} = 1/(2nv_y v_z t^2)$$
$$F(t) = 1 - \exp(-4nv_x v_y v_z t^3)$$
$$i_1(b) = \delta(b - 2v_x t)$$

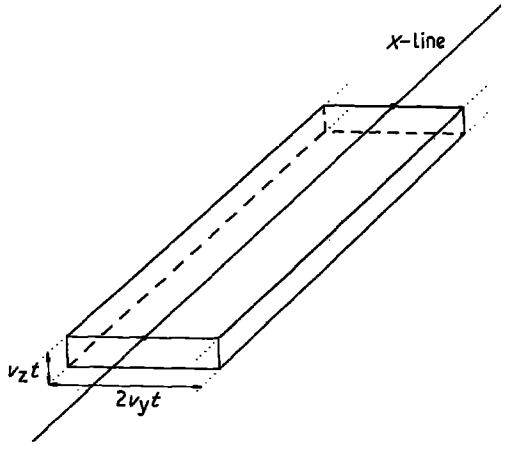

Figure 14 Half tube with the cross-section 0.5 × 0.1. The X-line is arranged in the surface x-y plane.

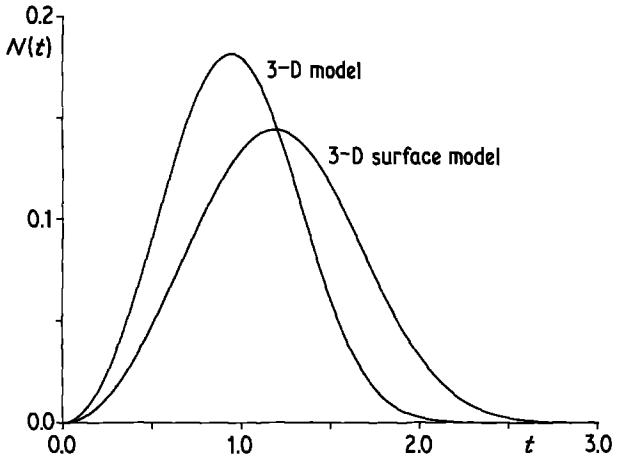

Figure 15 $N(t)$ along the X-line for the 3-D model and for the 3-D surface model.

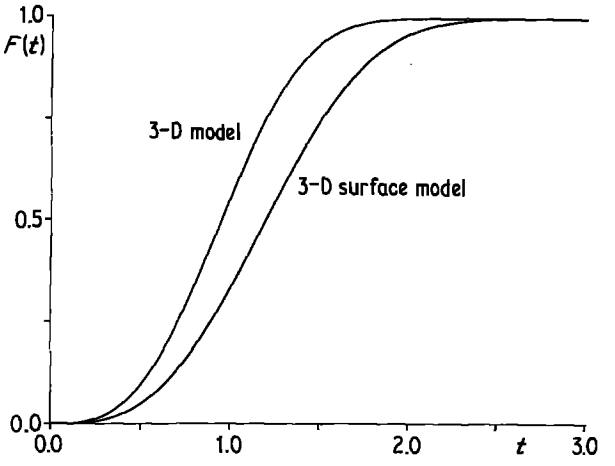

Figure 16 $F(t)$ for the 3-D model and for the 3-D surface model.

$$N_1(t) = 2nv_yv_zt^2 \exp(-8nv_xv_yv_zt^3)$$

$$N_2(t) = 2nv_yv_zt^2 \exp(-4nv_xv_yv_zt^3) \times [1 - \exp(-4nv_xv_yv_zt^3)]$$

$$i_2(b) = \frac{2nv_yv_zt^2}{\exp(-4nv_xv_yv_zt^3) - 1} \times \begin{cases} 0 & \text{for } 0 < b \leqslant 2v_xt \\ 1 & \text{for } 2v_xt < b \leqslant 2 \times 2v_xt \\ g(b;\, t,\, K) & \text{for } K2v_xt < b \leqslant (K+1)2v_xt \end{cases}$$

with $K = 2, 3, 4, \ldots$ and with

$$g(b;\, t,\, K) = 1 + \sum_{j=1}^{K-1} (-2nv_yv_zt^2)^j \exp(-j4nv_xv_yv_zt^3) \times \left\{ \frac{[b - (j+1)2v_xt]^j}{j!} + \frac{[b - (j+1)2v_xt]^{(j-1)}}{2nv_yv_zt^2\,(j-1)!} \right\}$$

$$\bar{b}(t) = \frac{\exp(4nv_xv_yv_zt^3) - 1}{2nv_yv_zt^2}$$

$$i(b) = \begin{cases} 0 & \text{for } b < 2v_xt \\ \exp(-4nv_xv_yv_zt^3)\,\delta(b - 2v_xt) & \text{for } b = 2v_xt \\ [1 - \exp(-4nv_xv_yv_zt^3)]\, i_2(b) & \text{for } b > 2v_xt \end{cases}$$

A comparison between the 3-D surface model and the 3-D model is given in dependence on time t in Fig. 15 for the mean number of A-phases (or B-phases) per unit length along the X-line, $N(t)$, and in Fig. 16 for the fraction transformed, $F(t)$.

5.3. Quantities along the Y-line and the Z-line

The interchange of the growth rates v_x, v_y, v_z, as given in Section 4.4., are used in Section 5.2. to obtain the results along the Y-line and along the Z-line.

6. 3-D model with growth rates depending on time

We will consider the 3-D model from Section 4.1., but now with $v_x(t)$, $v_y(t)$, and $v_z(t)$. In this model each unhindered grown B-grain is again a cuboid during the whole transformation, but the proportion of its three lengths depends on time t. This dependence may be caused by different stresses along different oriented interphase interfaces, which react to the rates of growth. With the abbreviation

$$V_i(t) = \int_{t=0}^{t} v_i(t)\,\mathrm{d}t \quad \text{for } i = x, y, z, \tag{33}$$

we obtain for the mean number of virtual nuclei per unit length along the X-line at time t

$$n_x = 2V_y2V_zn = 4nV_yV_z. \tag{34}$$

The length of each unhindered grown B-grain along the X-line at time t is given by

$$b_0 = 2V_x. \tag{35}$$

With the derivations in Sections 2 and 4 we obtain e.g.

$$W(t) = \exp(-8nV_xV_yV_z) \tag{36}$$

and

$$N(t) = 4nV_yV_z \exp(-8nV_xV_yV_z) \tag{37}$$

After derivation with respect to t we have, however,

$$\dot{N}(t) = 4n \exp(-8nV_xV_yV_z)[v_yV_y + V_yv_z - 8nV_yV_z(v_xV_yV_z + V_xv_yV_z + V_xV_yv_z)] \quad (38)$$

Section 4.3. and Equations 30 and 31 are true for the present case if we substitute $v_xt \to V_x$; $v_yt \to V_y$; $v_zt \to V_z$. ($\dot{N}$ is excepted and given in Equation 40.) After doing so, the quantities along the Y-line follow by replacement of V_x by V_y and V_y by V_x. (In $N(t)$ we have additionally to substitute $v_x \to v_y$ and $v_y \to v_x$.) The quantities along the Z-line follow by replacement of V_x by V_z and V_z by V_x from the quantities above. (In $N(t)$ we have additionally to substitute $v_x \to v_z$ and $v_z \to v_x$.)

Acknowledgements

We thank Dipl.-Phys. G. Schilling for the two microphotographs. The investigations were financially supported by the Land Nordrhein-Westfalen, FRG.

References

1. G. SCHILLING, Dipl.-Arbeit (Physik), Universität Düsseldorf, 1984.
2. S. A. SALTYKOV, "Stereometrische Analyse" (VEB Deutscher Verlag für Grundstoffindustrie, Leipzig, 1974).
3. R. T. DE HOFF and F. N. RHINES, "Quantitative Microscopy" (McGraw-Hill, New York, 1968).
4. E. E. UNDERWOOD, "Quantitative Stereology" (Addison Wesley, Reading, Massachusetts, 1970).
5. H. FREUD, "Handbuch der Mikroskopie in der Technik", Band III, Teil 2 (Umschau-Verlag, Frankfurt/Main, 1969).
6. G. E. W. SCHULZE, *J. Crystal Growth* **62** (1983) 7.
7. *Idem, Acta Metall.* **33** (2) (1985) 239.
8. A. RENYI, "Wahrscheinlichkeitsrechnung" (Deutscher Verlag der Wissenschaften, Berlin, 1977).
9. G. E. W. SCHULZE and H. KLINGER, unpublished result.

Received 14 November 1985
and accepted 10 January 1986